Virtual qualification of novel heat exchanger components with the image-based finite element method

Llion M. Evans[1,2], Triestino Minniti[2], Tom Barrett[2], Alexander von Müller[3], Lee Margetts[4]

[1]College of Engineering, Swansea University, Bay Campus, Swansea, SA1 8EN, UK, e-mail: llion.evans@swansea.ac.uk

[2]Culham Centre for Fusion Energy, Culham Science Centre, Abingdon, Oxon, OX14 3DB, UK, e-mail: triestino.minniti@ukaea.uk, tom.barrett@ukaea.uk

[3]Max-Planck-Institut für Plasmaphysik, Boltzmannstraße 2, 85748 Garching, Germany, e-mail: avonm@ipp.mpg.de

[4]School of MACE, University of Manchester, Manchester, M13 9PL, UK, e-mail: lee.margetts@manchester.ac.uk

Abstract

This paper presents the application of the image-based finite element method (IBFEM) to quantify the impact of micro-structure caused by manufacturing processes on the performance of fusion energy heat exchangers. The components, containing tungsten, were imaged with high-power lab-based X-ray CT and neutron CT. Volume data was converted into part-specific IBFEM meshes using the software ScanIP. The open source software ParaFEM was used to simulate the microstructurally faithful models using boundary conditions to simulate the extreme environment within a nuclear fusion reactor. By comparison with design-based simulations the impact of minor deviations from the design introduced during manufacturing were estimated. By digitally testing 'real' components, results can be interrogated through the sample's full volume. This provides more sophisticated information than pass/fail experimental tests which can be used to rate components in a manner similar to material purity for optimised usage.

Keywords: image-based modelling; finite element method; virtual characterisation; thermal conductivity; non-destructive testing; component qualification; manufacturing

1 Introduction

A growing field of activity within manufacturing is the use of industrial computational tomography (CT) to investigate deviations from the design caused during manufacturing. This is often achieved by a direct comparison of the component surfaces as described by the computer aided design drawing (CAD) and CT image, yielding a metrology measurement that highlights areas of difference. The shortcoming of this method is that it then relies on the operator to subjectively decide whether any observed deviations are significant. This usually relies on specifying a maximum allowable defect size which doesn't consider location or shape of defect. For example, a small defect in a critical location may have a greater detrimental effect on performance than a large one in a non-critical region. Image-based modelling is an advancement on this usage of industrial CT scanning by directly converting CT images into ultra-high resolution meshes. The meshes are used for part-specific computer simulations e.g. thermomechanical analysis with the image-based finite element method (IBFEM) or computational fluid dynamic (CFD) simulations. With this method it is possible to quantify the impact of features introduced during the manufacturing stage and not considered during design on the performance of each part individually.

This method has previously been used by the authors to investigate heat transfer across the joining interface between copper and carbon fibre composites in a heat exchange component for a nuclear fusion device [1]. Understanding the heat transfer across this interface is important because the thermally induced strains, caused by a large mismatch in the coefficient of expansion between the two materials, is a main contributor to component failure. Since the initial study, carbon fibre composites have been deselected as a candidate armour material by the fusion energy community mainly because of issues relating to tritium retention. The main material of interest for this region of the device is now tungsten, which is challenging to image with X-rays because of its relatively high attenuation levels. This paper presents an investigation into using a combination of high-power lab-based X-ray CT and neutron CT to produce images of fusion energy heat exchange components that have sufficient accuracy to produce IBFEM models to investigate the heat transfer across the tungsten-copper interface. Included in this paper is the first IBFEM analysis of tungsten heat exchange components for fusion. The focus of this work is on two novel designs manufactured by the Culham Centre for Fusion Energy (CCFE) and Max-Planck-Institut für Plasmaphysik (IPP).

2 Sample preparation

The most common nuclear fusion energy device is the tokamak. Within this, the divertor plays a key role as an exhaust for helium, the waste product of the fusion reaction. This component is therefore the one subjected to the greatest steady thermal load. During steady-state operation thermal fluxes are expected to be at least 10 $MW \cdot m^{-2}$. It is proposed that the divertor will consist of a series of flat armour tiles aligned in rows with one side being plasma facing [2]. In order to remain within operational temperature limits the components are actively cooled. This is achieved by connecting the tiles through their centres to a pipe carrying coolant (coined a monoblock). For ITER, the largest fusion device currently under construction, the monoblock will

use tungsten (W) for the armour with a copper alloy (CuCrZr) cooling pipe. The armour is bonded to the pipe to maintain thermal conduction, but a large thermal expansion coefficient mismatch between the W and CuCrZr causes high levels of stress within the part. Therefore, a functional compliant interlayer is used at the material interface to create a bond between the pipe and armour with improved longevity see Figure 1. For future devices, where it would be desirable to operate at higher thermal fluxes, alternatives designs are being investigated.

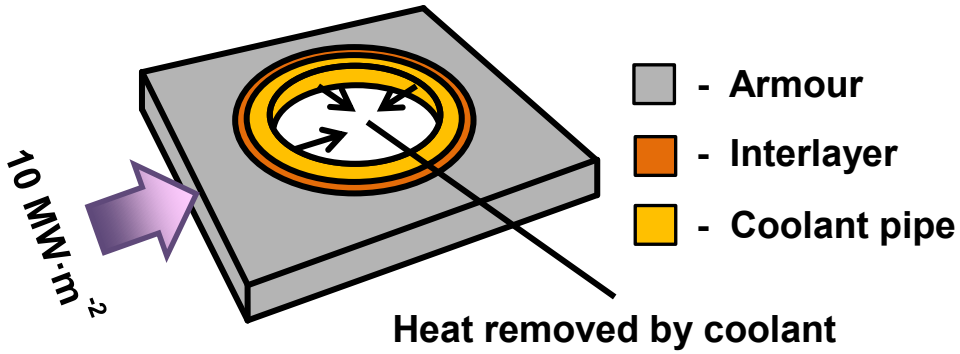

Figure 1: Schematic of divertor monoblock showing the main constituent regions and in-service loads.

This paper considers two such alternatives: Culham Centre for Fusion Energy thermal break concept monoblock (CCFE_MB) which uses geometric constructs to produce a more favourable thermal profile and Max-Planck-Institut für Plasmaphysik tungsten fibre / copper matrix composite coolant pipe (IPP_Wf-Cu) for reinforcement, as shown in Figure 2.

The 'CCFE_MB' sample was fabricated in several stages. Firstly, a bar of sintered tungsten is produced which is rolled to yield elongated grains whose longitudinal orientation are aligned such they shall not be parallel to the surface. The tungsten armour is then machined to shape before oxygen free high conductivity (OFHC) copper is directly cast into the internal hole. A stress relieving slit was cut into the plasma facing surface of the tungsten by electro-discharge machining (EDM). A drill is then used to machine the copper layer to leave the desired bonding layer thickness which is joined to an inner assembly using a two-stage vacuum braze process. Copper sleeves (for interlayer material) were first brazed to CuCrZr pipes and the geometric constructs (grooves) machined into the outer surface of the subsequent assembly. A second Cu-to-Cu braze process was performed where the W/Cu blocks are attached to the pipe/sleeve assembly to create the complete mock-up component. The final braze also included a precipitation hardening cycle. The braze filler material used was a 50:50 Au-Cu foil, known commercially as Orobraze 970, which had a thickness of 25 µm and was wrapped around the inner part three times before bonding. For more details on the design and manufacture of the monoblock see [3].

For the 'IPP_Wf-Cu' sample, the W fibre preform used was manufactured by means of sequential circular mandrel overbraiding. The raw material used were drawn potassium (K) doped W fibres with a nominal diameter of 150 µm. The resulting preform comprised 5 braided layers which exhibited a regular 2/2 twill weave repeat pattern. The W_f-Cu composite material was then produced by infiltrating the braided preform with liquid Cu. Eventually, the infiltrated composite was machined to final dimensions (inner diameter: 10 mm, wall thickness: 1.5 mm) and specimens with an axial length of 10 mm were cut. For further detail on the manufacturing and the motivation for interest in W_f-Cu materials for this application see [4].

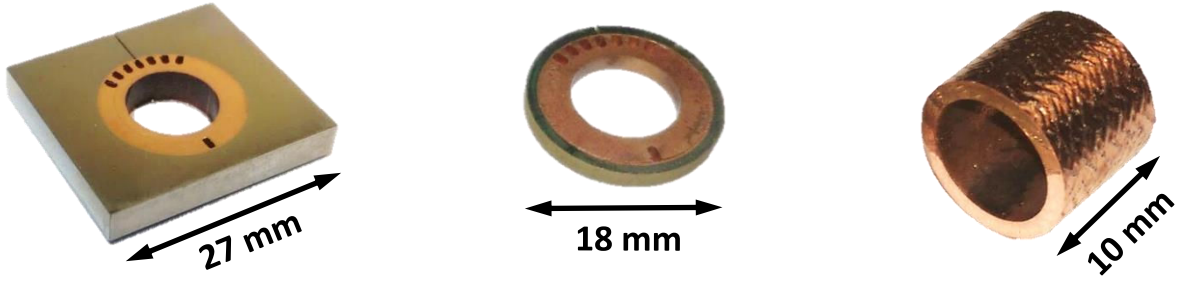

(a) (b) (c)

Figure 2: Two sample types used for this work: (a) Culham Centre for Fusion Energy thermal break concept monoblock (CCFE_MB), (b) region of interest (ROI) sub-sample from CCFE_MB and (c) Max-Planck-Institut für Plasmaphysik tungsten fibre / copper matrix coolant pipe (IPP_Wf-Cu)

Because tungsten's has extremely high X-ray attenuation levels, a sufficiently long tungsten attenuation path would reduce the X-ray signal source such that it would not be possible to gather sufficient data to perform a volumetric reconstruction. To reduce the attenuation path length a 'region of interest' (ROI) sample was produced from the CCFE_MB sample by using electro discharge machining (EDM) to remove all but a 0.5 mm layer of tungsten armour around the coolant pipe, see Figure 2 (b). The

aim was to leave a tungsten layer sufficiently thick such that the EDM cut would not affect the material interfaces but thin enough to allow full X-ray penetration.

2 Method

Industrial X-ray CT is a well-established technique, therefore detailed methodology and hardware specifications can readily be found elsewhere e.g. [5], [6]. X-ray CT scanning used a Nikon 225 with the machine parameters as shown in Table 1.

Because the full CCFE_MB sample contained a relatively large volume of tungsten it was not scanned via X-ray CT, however the ROI equivalent sample was. To further reduce the attenuation path length, this sample was scanned at a ~45° tilt angle.

The IPP composite pipe was scanned before the addition of the tungsten armour, therefore the only tungsten content was that of the 150 μm diameter fibres, the remaining volume was copper matrix. This sample was scanned with the centreline of the pipe along the manipulator stage's centre of rotation.

Reconstruction of the 3D volume from 2D radiographs was completed using CT Pro V3.1 (Nikon Metrology NV, Tring, Hertfordshire, UK).

Table 1 : X-ray tomography scanning parameters.

Sample	Voltage (kV)	Current (μA)	Filter (mm)	Acquisition time (s)	Number of projections	Tilt angle (°)
CCFE_MB	N/A	N/A	N/A	N/A	N/A	N/A
CCFE_MB_ROI	220	80	Cu, 0.5	1.0	3142	45
IPP_Wf-Cu	200	220	Cu, 2.0	0.5	2616	0

Because neutrons are significantly more penetrating it was possible to image the full monoblock sample, CCFE_MB, in addition to the others. Neutron tomography was performed at IMAT, ISIS, Rutherford Appleton Laboratory, STFC, UK [7]–[9]. The method for neutron scanning is similar to that of X-ray tomography. The main difference between the two scanning setups used here was that X-ray CT used a cone angle beam whereas the neutron beam was quasi-parallel, other scan parameters are shown in Table 2. The CCFE_MB_ROI and IPP_Wf-Cu samples were scanned together by stacking one on top of the other with a 0° tilt angle. To reduce the attenuation path length through the CCFE_MB sample it was scanned at a ~45° tilt angle. For more details on the neutron scan setup see [10].

Reconstruction of the 3D volume from 2D radiographs was completed with a standard filtered back-projection algorithm using Octopus Imaging Software (XRE NV, Gent, Belgium).

Table 2 : Neutron tomography scanning parameters.

Sample	Acquisition time (s)	Number of projections	Tilt angle (°)
CCFE_MB	30	1333	45
CCFE_MB_ROI	30	707	0
IPP_Wf-Cu	30	707	0

Volume segmentation and IBFEM mesh generation used ScanIP and the +FE module, part of the Simpleware suite of programmes, version 7 (Synopsys Inc., Mountain View, CA, USA). Because of the levels of noise and artefacts in the images automated greyscale thresholding techniques were not well suited for segmentation. Rather a range of semi-automated techniques were used including the flood-fill, cavity fill, island removal, manual paint tools and a recursive Gaussian smoothing filter. Linear 4-node tetrahedral elements were selected for meshing.

Computational expense (i.e. number of calculations) increases with the number of elements. To reduce this number, the meshing software was set to use a finer mesh around areas of microstructural detail but a coarser mesh in the bulk. However, to faithfully represent the micro-structure of the components, the IBFEM models still require meshes that contain a number of finite elements which is several orders of magnitude greater than design-based models from idealised CAD.

Commercial FEM software packages cannot solve these large and complex simulations on desktop PCs. Furthermore, commercial FEM software is not suited to supercomputers because they do not make efficient use of parallelisation. Therefore, the open source solver ParaFEM, developed by the authors [11], was used because it has previously been shown to scale well on parallel computing architectures i.e. the time to solve almost halves as the number of computational cores doubles.

In order to simulate the image-based models under a relevant steady-state scenario the boundary conditions as shown in Figure 1 were used. That is, a thermal flux of 10 MWm^{-2} was applied to the upper surface of the armour to represent the plasma, an initial temperature of 150 °C and a non-linear negative flux on the inner pipe wall to represent the temperature dependent cooling. The cooling thermal flux was calculated using the FILM-2000 software [12]. A 150 °C coolant with velocity of 16 m/s at a

pressure of 5 MPa was used. Visualisation and analysis of results was performed using ParaView, version 4.4 64-bit (Kitware Inc., Clifton Park, New York, USA).

Temperature dependent material properties were used taking values for W, Cu, Au and CuCrZr from the ITER materials properties handbook (IMPH) [13]. For the 50:50 Cu and Au braze layer, a simplistic approximation was made by averaging the values for Cu with Au.

3 Results

The volume of the constituent parts of the samples was calculated geometrically and is shown in Table 3. Because the samples had an approximately 1:1 aspect ratio, the calculated volumes give an indication of the level of attenuation which could be expected from the samples. It can be seen that the W volume for the CCFE_MB_ROI and IPP_Wf-Cu are comparable, with the IPP_Wf-Cu sample containing ~65 % more Cu. The full monoblock sample (CCFE_MB) contains significantly more W, hence why it was only scanned by neutron CT and not X-ray CT.

Table 3 : Volume of constituent parts from samples as calculated geometrically.

Sample	W Volume (mm^3)	Cu Volume† (mm^3)
CCFE_MB	1684	594
CCFE_MB_ROI	55	297
IPP_Wf-Cu	54	488

† Combined volume of pure Cu and Cu alloys.

Figure 3 demonstrates that both X-ray and neutron techniques were capable of imaging the CCFE_MB_ROI sample despite W being a relatively high attenuator of X-rays and neutrons. X-ray CT yielded an image with accuracy sufficiently high that features of 60 µm or greater could be resolved (e.g. the 75 µm thick braze layer). For neutron CT, features of 250 µm and greater were resolvable. The image resolution impeded measurement of the braze layer however, it was clearly visible at the layer interfaces. In the neutron image there was a measurable difference in the greyscale levels of the inner CuCrZr coolant pipe and outer Cu functional interlayer which was not observed in the X-ray image. Although the X-ray image provided better resolution of the ROI sample, the main reason for using neutron tomography was to investigate non-destructive testing of full monoblocks. This was achieved successfully with neutron tomography, see Figure 4. This yielded a similar resolution to the ROI sample, i.e. resolving features of 250 µm and greater, due to the quasi-parallel beam setup.

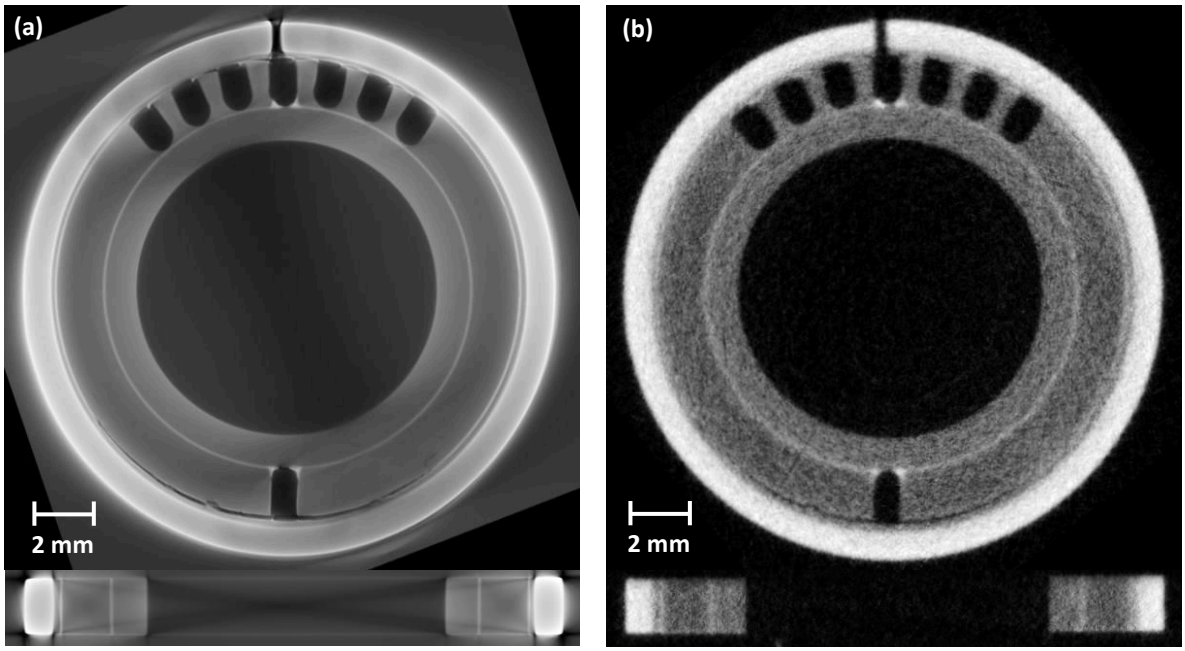

Figure 3: Example cross sectional tomography data slices from the xy (top) and xz (bottom) planes for the CCFE_MB_ROI sample with a comparison of X-ray (left) vs. neutron (right) tomography imaging results.

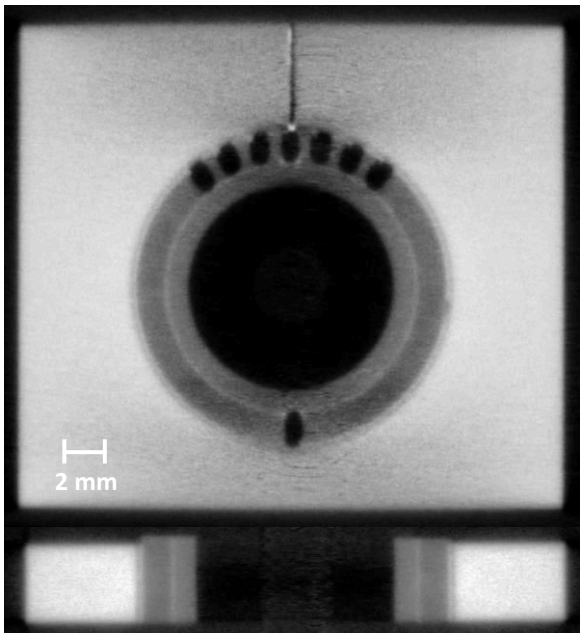

Figure 4: Example cross sectional neutron tomography data slices from the xy (top) and xz (bottom) planes for the CCFE_MB samples.

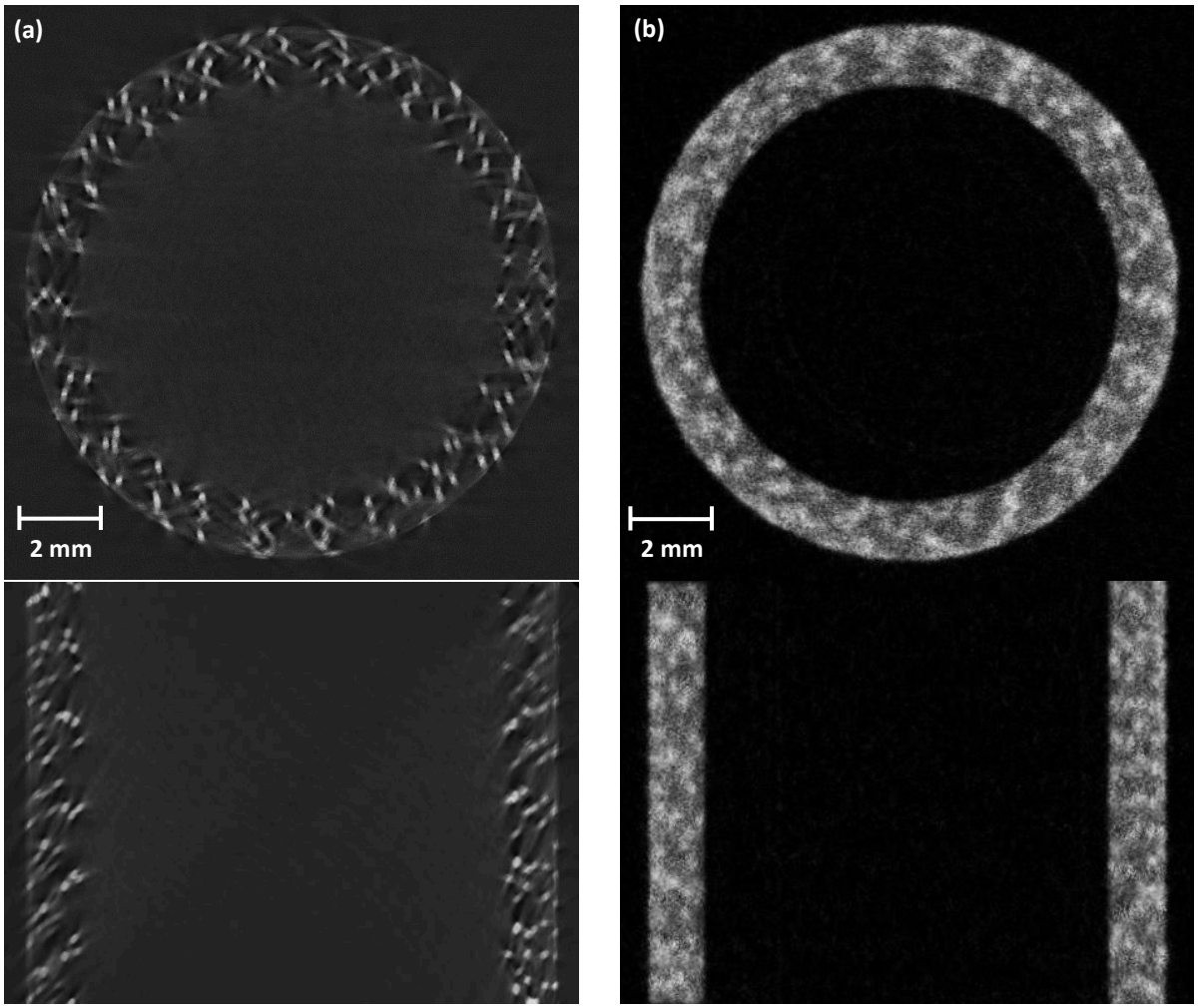

Figure 5: Example cross sectional tomography data slices from the xy (top) and xz (bottom) planes for the IPP_Wf-Cu sample with a comparison of X-ray (left) vs. neutron (right) tomography imaging results.

For the fibre composite sample (IPP_Wf-Cu), the X-ray image had a voxel width of 12.6 µm which was sufficient to distinguish the individual composite fibres which had a diameter of 150 µm. However, there was low observable contrast in greyscale values between the Cu matrix and the surrounding background air, see Figure 5 (a). Additionally, streaking artefacts from the W fibres were prominent. This led to poor definition of the sample boundaries and meant that metrology or investigations of material interfaces were effectively impossible. However, what could be achieved was accurate location of the fibre centrelines to identify deviations from the ideal weave pattern. The neutron image resolution was sufficient to resolve individual fibres, see Figure 5 (b). Greyscale contrast was improved, and no streaking artefacts were observed leading to an image useable for metrology but with insufficient resolution to investigate the fibre-matrix interfaces.

Key to this work was the use of CT images to create IBFEM meshes. For the monoblock, no features of interest were observed in the bulk of the W armour from the neutron image. Therefore, it was decided that it would be preferable to use X-ray CT image of the ROI sample as this provided the best resolution at the material interfaces where deviation from design was observed. Because bulk of the W armour had been cut from the ROI sample, it had to be digitally replaced to create an IBFEM model of the whole monoblock from the ROI image. This method created a hybrid IBFEM-CAD mesh, with IBFEM data faithfully recreating the microscale of the material interfaces and geometric constructs but idealised CAD drawing for the remaining W armour as shown in Figure 6 (a). For the IPP_Wf-Cu sample the neutron image presented the best data. Similarly, the tungsten armour was added with CAD but this time assuming an idealised interface between the pipe and armour. This was method was chosen because the feature of interest was the impact of individual fibre placement on global performance. For this sample three armour tiles were digitally added equidistant along the pipe length, see Figure 7 (a).

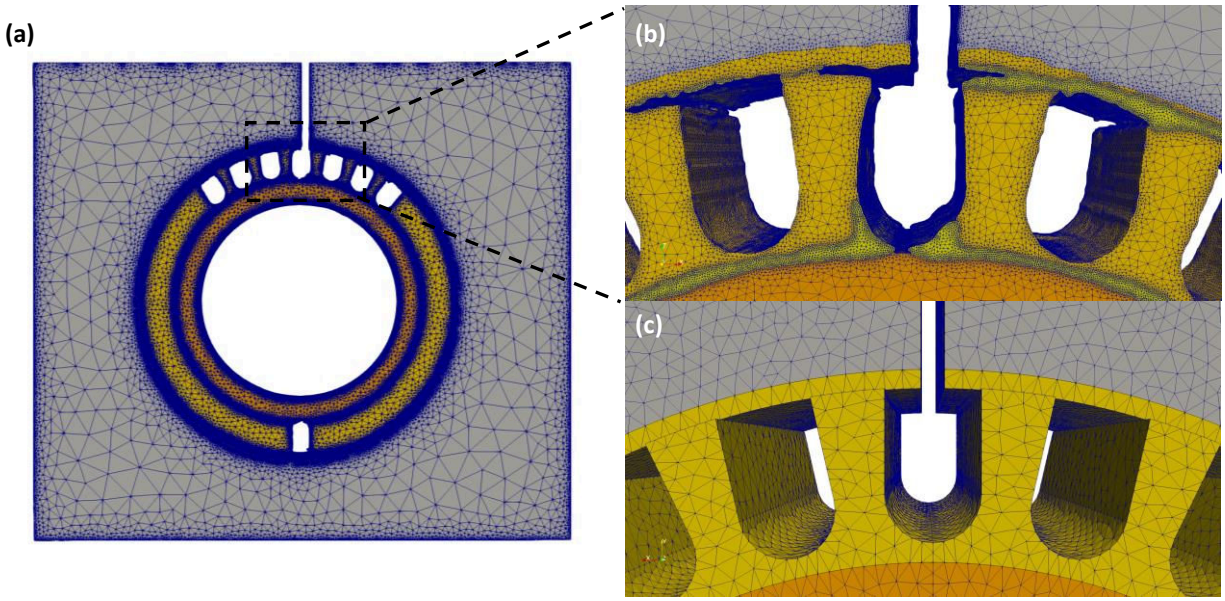

Figure 6: (a) Image-based finite element method (IBFEM) mesh created from X-ray tomography image of 'region of interest' CCFE Thermal break sample, W armour which was removed by EDM has been replaced digitally. (b) Zoomed in region showing material interface for IBFEM mesh. (c) Idealised CAD mesh from same zoomed in region.

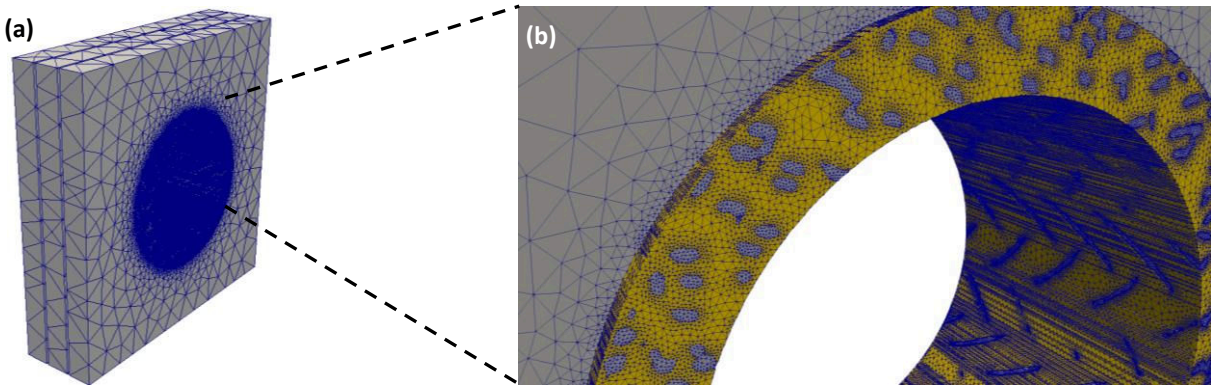

Figure 7: Image-based model of W_f/Cu pipe, including individually meshed fibres, with the addition of 3 W armour tiles.

The FE meshes created consisted of 6.1 and 19.3 million tetrahedral elements for the CCFE_MB_ROI and IPP_Wf-Cu samples, respectively. These are shown in Figure 6 and Figure 7 along with zoomed in regions demonstrating the microstructural detail included inherently by this method but omitted in CAD models (e.g. debonding within the braze layer). To validate the meshes, the volumes of constituent parts were checked against geometric calculations. Differences were found to be negligible. Additionally, the elements were checked against standard 'quality' metrics such as skewness. It was found that a very small percentage of elements were outside the desired thresholds (less than 0.001%). Because of the meshes fine resolutions it is expected that any impact on numerical results will be extremely localised and minimal. Therefore, it was considered that the meshes were of adequate quality for FE simulations.

To make a relative comparison between the simulation results it is worth investigating some key values. Table 4 shows the values for maximum temperature, the average temperature on the plasma facing surface (PFS) of the armour, the maximum temperature and maximum Von Mises stress in the coolant pipe. These values were selected because of their relevance to engineering design acceptance criterion. Because the CCFE_MB_CAD and CCFE_MB_IBFEM results are based on the same design, it is worth firstly comparing these results. The average PFS temperatures are almost identical, whereas greater differences are seen in the peak values (particularly Von Mises stress). The higher 'peaks' observed in the IBFEM model were found to be extremely localised due to microfeatures (e.g. a micron-scale piece of braze at material interfaces). If conventional 'design rules' decisions were used, such as Structural Design Criteria for In-vessel Components (SDC-IC), based on the high stress results of this purely elastic simulation the component's lifespan would be estimated at less than 10 cycles. However, from experimental data [3] it is known that the component was tested to 100 cycles with little visible damage. The lower stresses in the less detailed CAD simulation yield longer SDC-IC lifecycle estimates. This is because 'design rules' have been written to be used conservatively with idealised CAD-based simulations. For image-based models, localised maxima often occur where very small features act as stress concentration zones. In practicality, these would plastically deform or fracture after the first cycle therefore relieving stress for subsequent cycles. As long as these are not initiation sites for further defect propagation they are likely to have minimal impact on the lifecycle length. Although IBFEM more closely mimics 'real world' performance, conventional 'design rules' cannot be considered well suited for assessing results from image-based FEM analyses. Further work is needed to investigate the effect of localisation of peak values in order to propose amended 'design rules' which accounts for the global impact and thus suitable for IBFEM.

Table 4 : Key values from simulation results of various monoblocks under 10 MW/m^2 thermal load.

Model	T_{max} (°C)	T_{avg} on PFS* (°C)	T_{max} in pipe (°C)	Max Von Mises in pipe (MPa)
CCFE_MB_CAD	1036	953	331	1.48E+08
CCFE_MB_IBFEM	1423	951	359	8.23E+09
IPP_Wf-Cu	1198	902	355	3.19E+09

*Plasma Facing Surface

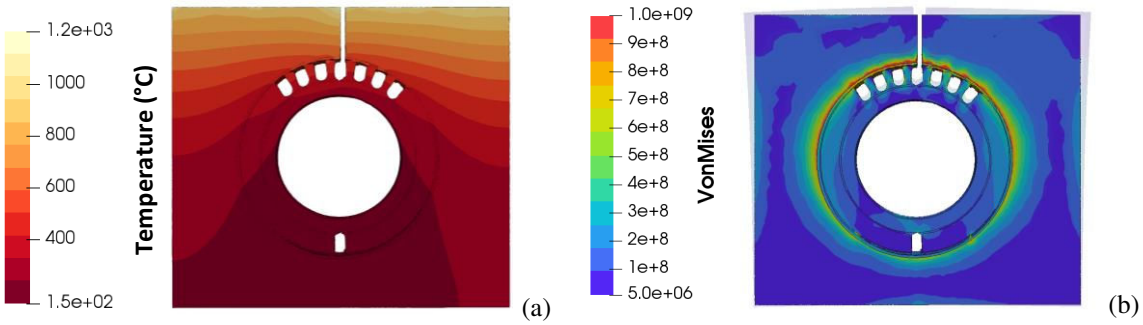

(a) (b)

Figure 8: Results from thermal IBFEM analysis showing (a) non-symmetric temperature profile in CCFE_MB sample due to geometric constructs not being perfectly central and (b) Von Mises thermally induced stress with addition of displacement warp outline (factor of x20).

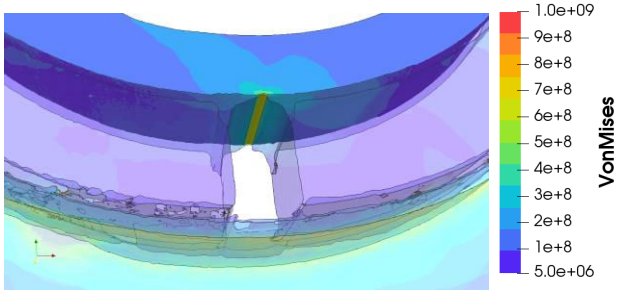

Figure 9: Closeup of CCFE_MB showing stress concentration in the CuCrZr pipe in the vicinity of a gap in the braze.

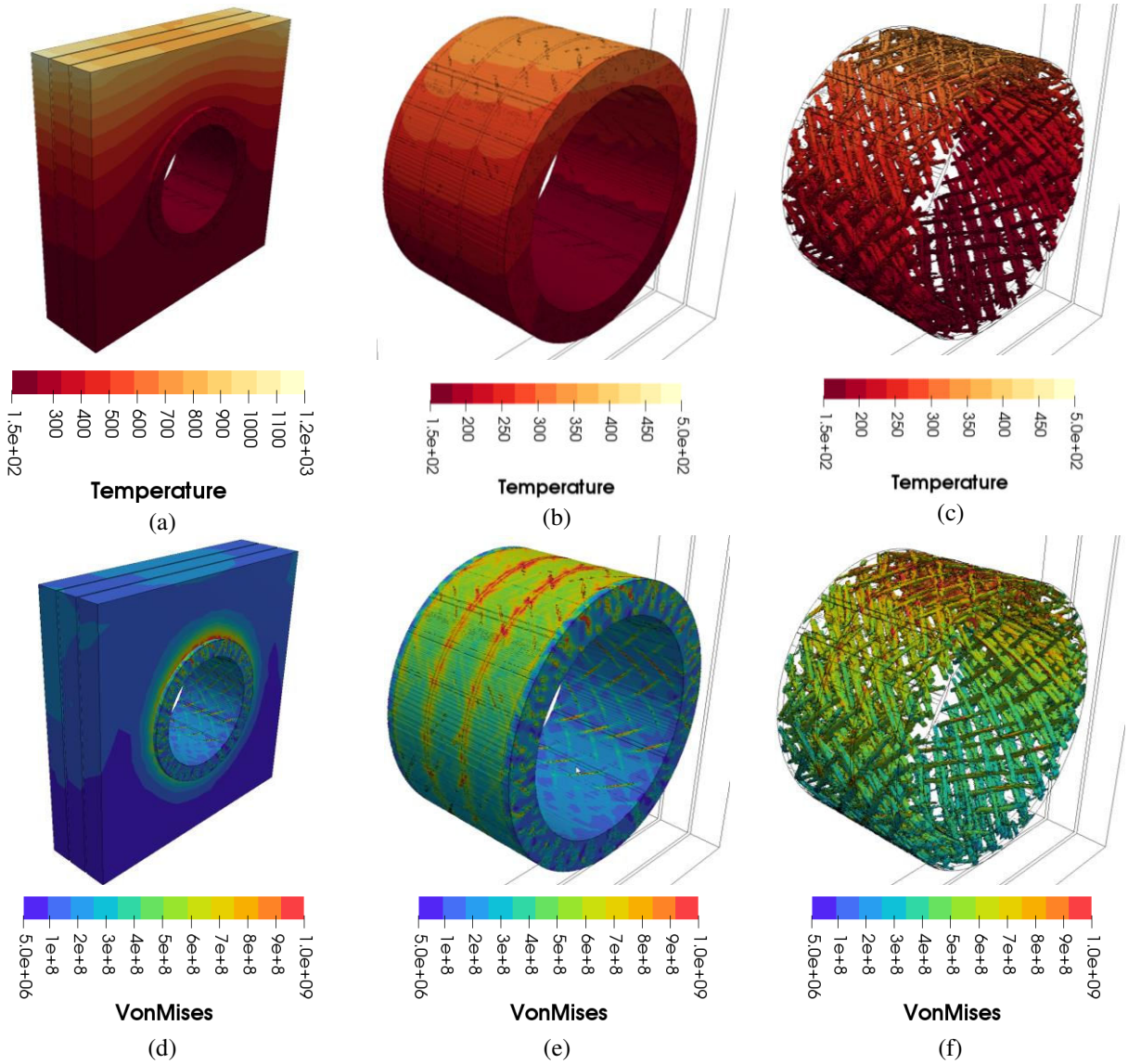

Figure 10: Results for (a-c) temperature and (d-f) Von Mises stress distribution for an IBFEM simulation of the IPP W_f/Cu composite pipe with three W armour tiles added. This highlights the variation observed along the length of the pipe and the value of having part-specific models to calculate this variation. (a & d) show results for the whole assembly, (d & e) and (c & f) are visualisation of results in the composite pipe and fibres alone, respectively.

Because the CCFE and IPP designs are of such a different nature it is not that useful to make a direct comparison to select the 'best' performer because they could be further optimised for specific functions. Having said this, it can be observed that the results for the two IBFEM simulations are relatively similar but with the IPP_Wf-Cu yielding consistently lower temperature and stress values.

It is useful to make more qualitative observations and comparisons between the IBFEM simulations with their idealised CAD counterparts. Although the global temperature and stress fields were of the same order of magnitude, the differences related to the non-symmetric behaviour inherent in a non-idealised geometry. For example, the CCFE_MB temperature profile slightly differs on the left- and right-hand side, as shown in Figure 8 (a). This is seemingly due to the geometric constructs in the copper interlayer not being perfectly central and a small region of debonding at the material interface being asymmetric. For the IPP_Wf-Cu model, the temperature profile in each armour tile is slightly different due to the exact location of the fibres within the coolant pipe causing variations in conductivity paths, see Figure 10 (a). Neither of these effects would be included in CAD based simulations but the minor deviations are shown to have had a quantifiable impact on performance. The added value of the IBFEM results is that they gave more accurate localised results by including microstructural detail. Figure 9 highlights a stress concentration zone in the coolant pipe where a gap has appeared in the braze layer. This is observed elsewhere in the model near regions of poor bonding. Figure 10 (e) and (f) show the stress in the fibres and matrix of the composite material caused by the mismatch of thermal expansion coefficient in a component being thermally loaded.

The implications of this application of industrial CT ar far reaching. Current practice is often to use CT images to identify defects or deviations from design then subjectively decide the significance of the discovered feature. The deciding factor for this approach is often the size of the defect, however a small defect in a critical region can have a greater impact on performance than a large one in a non-critical region. Additionally, defect shape can have a large effect on the impact it has. IBFEM gives quantifiable value to iCT by simulating the impact of each specific defect and deviation by accounting for their size, shape and location. This improves on simplistic pass/fail testing by estimating part-specific performance of components in relation to the idealised design. This approach enables components to be sorted into performance bands analogous to material purity. This can lead to efficiency gains by reduced scrappage or by optimising component use e.g. positioning of parts within a large assembly.

4 Conclusions

The image-based finite element method (IBFEM) was used to simulate the impact on performance of microscale defects and deviations from design of a heat exchange components for a fusion energy device. This method was applied by using X-ray and neutron CT to image the volume of the component, then this 3D image was converted directly into a high-resolution engineering simulation which included features such as micro-pores at material interfaces that have a non-negligible effect on performance but are not considered in simulations during the design phase. Two components were investigated, a novel design from Culham Centre for Fusion Energy (CCFE) which uses geometric constructs to engineer a preferable temperature profile and a novel fibre composite material from Max-Planck-Institut für Plasmaphysik (IPP) to create a coolant pipe with improved strength. The CCFE component was found to exhibit non-symmetrical performance due to micro-features and the IPP component had varying performance along the length of the pipe due to precise fibre positioning. Neither of these effects are predicted by CAD-based simulations. This work demonstrated the benefit of IBFEM to estimate part specific performance of components ‘as manufactured’ rather than ‘as designed’.

Acknowledgements

This work has been carried out within the framework of the EUROfusion Consortium and has received funding from the Euratom research and training programme 2014-2018 under grant agreement No 633053, from the RCUK Energy Programme [grant number EP/I501045] and EPSRC [grant number EP/R012091/1]. To obtain further information on the data and models underlying this paper please contact PublicationsManager@ukaea.uk. The views and opinions expressed herein do not necessarily reflect those of the European Commission. This work made use the HPC resources of The Hartree Centre (project fusionFEM) made available within the Distributed European Computing Initiative (DECI-12) by the PRACE-2IP, receiving funding from the European Community’s Seventh Framework Programme (FP7/2007-2013) under grant agreement RI-283493. Access to the Archer UK National Supercomputing Service was provided by EPSRC through projects EP/N026136/1 and e515 “GEMS: Geometric Modelling of Solids”.

References

[1] Ll. M. Evans, L. Margetts, V. Casalegno, L.M. Lever, J. Bushell, T. Lowe, A. Wallwork, P. Young, A. Lindemann, M. Schmidt, P.M. Mummery, “Transient thermal finite element analysis of CFC–Cu ITER monoblock using X-ray tomography data,” Fusion Eng. Des., vol. 100 (2015) pp. 100–111.

[2] M. Merola and G. Vieider, “On the use of flat tile armour in high heat flux components,” J. Nucl. Mater., vol. 258–263 (1998) pp. 672–676.

[3] M. Fursdon, T. Barrett, F. Domptail, Ll.M. Evans, N. Luzginova, N.H. Greuner, J-H. You, M. Li, M. Richou, F. Gallay, “The development and testing of the thermal break divertor monoblock target design delivering 20 MW m −2 heat load capability,” Phys. Scr., vol. T170 (2017) p. 14042.

[4] A. v. Muller, D. Ewert, A. Galatanu, M. Milwich, R. Neua, J.Y. Pastor, U. Siefken, E. Tejado, J.H. You, “Melt infiltrated tungsten–copper composites as advanced heat sink materials for plasma facing components of future nuclear fusion devices,” Fusion Eng. Des., vol. 124 (2017) pp. 455–459.

[5] British Standard, “Non destructive testing - Radiation methods - Computed tomography - Part 2: Principle, equipment and samples,” (2011) pp. 1–21.

[6] British Standard, “Non destructive testing — Radiation methods — Computed Tomography Part 3: Operation and interpretation,” (2011).

[7] T. Minniti, W. Kockelmann, G. Burca, J.F. Kelleher, S. Kabra, S.Y. Zhang, D.E. Pooley, E.M. Schooneveld, Q. Mutamba, J. Sykora, N.J. Rhodes, F.M. Pouzols, J.B. Nightingale, F. Aliotta, L.M. Bonaccorsi, R. Ponterio, G. Salvato, S. Trusso, C. Vasi, A.S. Tremsin, G. Gorini, “Materials analysis opportunities on the new neutron imaging facility IMAT@ISIS,” J. Instrum., vol. 11, no. 3 (2016) pp. C03014–C03014.

[8] W. Kockelmann, G. Burca, J.F. Kelleher, S. Kabra, S. Zhang, N.J.Rhodes, E.M. Schooneveld, J. Sykora, D.E. Pooley, J.B. Nightingale, F. Aliotta, R.C. Ponterio, G. Salvato, D. Tresoldi, C. Vasi, J.B. McPhate, A.S.Tremsin, “Status of the Neutron Imaging and Diffraction Instrument IMAT,” in Physics Procedia, vol. 69 (2015) pp. 71–78.

[9] T. Minniti, K. Watanabe, G. Burca, D. E. Pooley, and W. Kockelmann, “Characterization of the new neutron imaging and materials science facility IMAT,” Nucl. Instruments Methods Phys. Res. Sect. A Accel. Spectrometers, Detect. Assoc. Equip., vol. 888 (2018) pp. 184–195.

[10] Ll. M. Evans, T. Minniti M. Fursdon M. Gorley T. Barrett F. Domptail E. Surrey W. Kockelmann A.v. Müller F. Escourbiac A. Durocher, "Comparison of X-ray and neutron tomographic imaging to qualify manufacturing of a fusion divertor tungsten monoblock," Fusion Eng. Des., vol. 134 (2018), pp. 97–108.
[11] I. M. Smith, D. V. Griffiths, and L. Margetts, Programming the Finite Element Method, 5th ed. Chichester: Wiley, 2013.
[12] T. D. Marshall, D. L. Youchison, and L. C. Cadwallader, "Modeling the Nukiyama curve for water cooled fusion divertor channels", Fusion Technol., vol. 35 (2001) pp. 8-16.
[13] J. W. Davis and P. D. Smith, "ITER materials properties handbook," J. Nucl. Mater., vol. 237, no. 96 (1996) pp. 1593–1596.